ACS Photonics

Article

pubs.acs.org/journal/apchd5

Nanometric Resolved Luminescence in h-BN Flakes: Excitons and Stacking Order

Romain Bourrellier,[†] Michele Amato,[†,‡,§] Luiz Henrique Galvão Tizei,[†] Christine Giorgetti,[‡] Alexandre Gloter,[†] Malcolm I. Heggie,[∥] Katia March,[†] Odile Stéphan,[†] Lucia Reining,[‡] Mathieu Kociak,[†] and Alberto Zobelli*[,†]

[†]Laboratoire de Physique des Solides, Université Paris-Sud, CNRS UMR 8502, F-91405, Orsay, France

[‡]Laboratoire des Solides Irradiés, Ecole Polytechnique, Palaiseau and European Theoretical Spectroscopy Facility (ETSF), Route de Saclay, F-91128 Palaiseau, France

[§]Institut d'Electronique Fondamentale, Université Paris-Sud, CNRS, 91405 Orsay, France

[∥]Department of Chemistry, University of Surrey, Guildford GU2 7XH, United Kingdom

Supporting Information

ABSTRACT: The strong excitonic emission of hexagonal boron nitride (h-BN) makes this material one of the most promising candidate for light emitting devices in the far ultraviolet (UV). However, single excitons occur only in perfect monocrystals that are extremely hard to synthesize, while regular h-BN samples present a complex emission spectrum with several additional peaks. The microscopic origin of these additional emissions has not yet been understood. In this work we address this problem using an experimental and theoretical approach that combines nanometric resolved cathodoluminescence, high resolution transmission electron microscopy and state of the art theoretical spectroscopy methods. We demonstrate that emission spectra are strongly inhomogeneous within individual few layer flakes and that additional excitons occur at structural deformations, such as faceted plane folds, that lead to local changes of the h-BN layers stacking order.

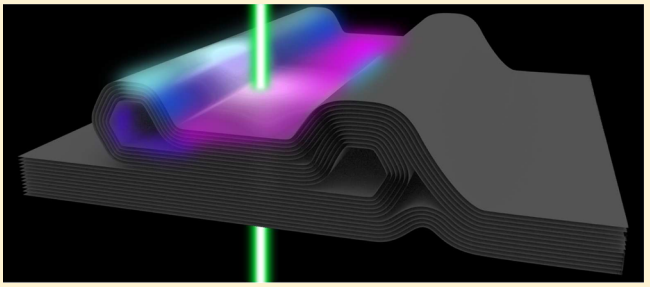

KEYWORDS: *boron nitride, cathodoluminescence, excitons, theoretical spectroscopy, electron microscopy*

The most energetic radiations that can propagate in air without significant attenuation are in the far UV region (4.4−6.3 eV). There is thus a strong technological interest in efficient light emitting devices in this spectral window for applications going from microbial sterilization to surgery tools. The well-known drawbacks of standard UV lamps (poor lifetime, limited output powers, chemical hazards) have provided strong motivations to search for a convenient solid state alternative. Whereas AlN based LEDs emitting at 5.9 eV have been already built, their low emission efficiency, due to a high density of defects quenching the emission, strongly limits their technological potential.[1,2] In the last years, hexagonal boron nitride (h-BN) and derived nanoforms (BN nanotubes, flakes) emerged as a promising alternative candidate for optoelectronic applications in the far UV region.[3−6] An efficient BN based ultraviolet (UV) light emitter in the 5.3−5.9 eV energy range has been recently obtained using accelerated electrons as the pumping source.[7] For the design of future h-BN devices it is fundamental to have an in-depth description and understanding of the complex luminescence of this material.

Theoretical and experimental works have demonstrated that the emission spectrum of h-BN is dominated by a Frenkel type exciton at 5.75 eV.[3,4,8,9] However, a single peak emission appears only in high quality crystals that can be obtained only in a limited amount through high pressure and high temperature synthesis processes.[10] Common h-BN samples present a more complex emission spectrum with a series of sharp emissions close to the main exciton in the 5.3−5.9 eV energy range. An additional broad emission occurs within the electronic band gap in the energy range 3.2−4.5 eV on which a series of three sharp lines might be superposed, depending on the BN sample purity.[11,12]

The origin of this complex emission pattern is still controversial and it has been attributed to the presence of unidentified structural defects. Impurities have been proposed to be responsible for emission lines in the band gap[12] and generic dislocations or grain boundaries to be at the origin of emission lines near the free exciton. The latter hypothesis has been suggested by the appearance of additional emission peaks when a pristine perfect crystal was deformed by a limited mechanical strain.[13,14] Furthermore, it has been shown through submicrometric emission maps obtained by cathodoluminescence (CL) filtered images that the standard exciton is

Received: April 29, 2014
Published: July 25, 2014

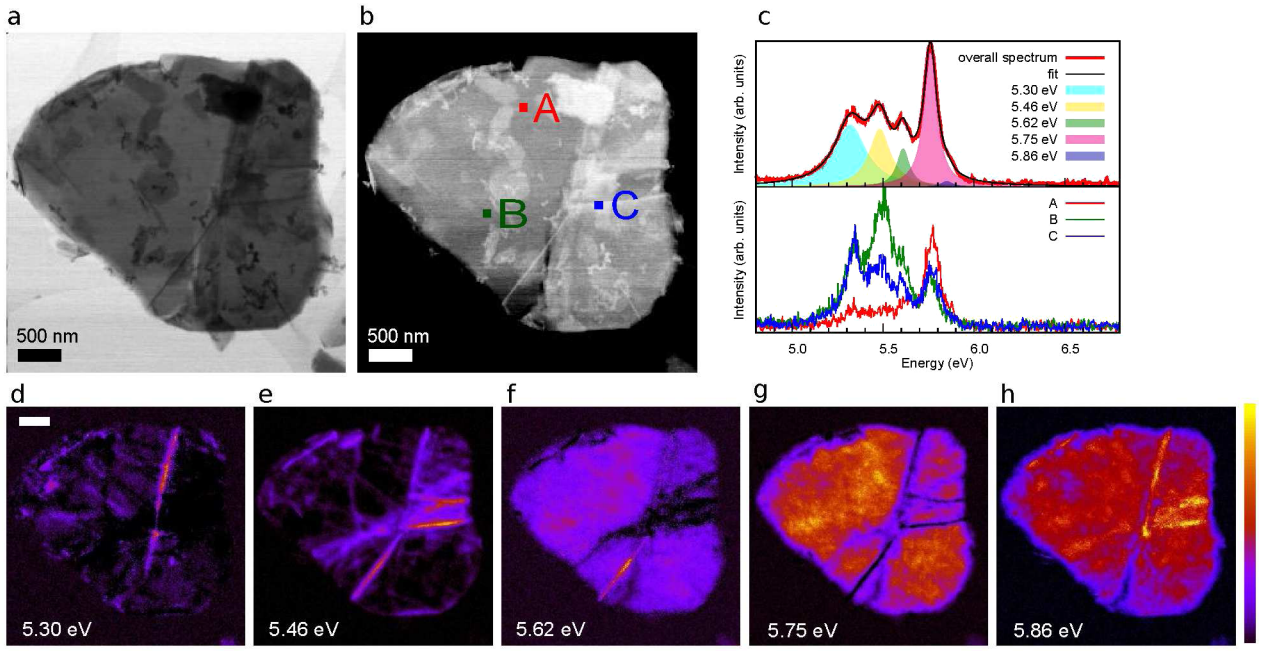

Figure 1. (a) Bright field and (b) dark field images of an individual BN flake. (c) Overall emission spectrum of the flake and individual spectra taken at specific probe positions indicated in panel b. (d–h) Emission maps for individual emission peak. Intensity is normalized independently within each individual map.

homogeneous in a h-BN crystallite whereas additional peaks present some spatial localization.[6,15,16] However, research conducted in the last ten years has not yet been able to correlate the optical properties of h-BN with the microscopic structure of defects. Here we address this fundamental question by adopting a theoretical and experimental approach combining few nanometer resolved cathodoluminescence techniques[17] with high resolution transmission electron microscopy images and state of the art quantum mechanical simulations. We show how additional excitonic emissions are associated with changes in the layer stacking order and how these structures can appear at local layers folds.

RESULTS AND DISCUSSION

h-BN flakes with an average lateral size of about 2–3 μm and thickness from a few nanometers down to the monolayer were obtained by chemical exfoliation through ultrasonication in isopropanol. Luminescence within individual h-BN flakes was investigated at a nanometric resolution through cathodoluminescence hyperspectral imaging. Individual particles were scanned by a 1 nm electron probe in a scanning transmission electron microscope (STEM) and a full emission spectrum in the 3.0–6.0 eV energy range was acquired at each probe position together with a bright field and a high angle annular dark field image, HAADF (a full emission spectrum is shown in Supporting Information, Figure 1). In this work we will focus on excitonic emissions in the 5.3–5.9 eV energy range, the most interesting spectral region for optical applications,[7] leaving to future discussion additional emissions appearing occasionally in the middle of the band gap.

In Figure 1a,b we present bright field and HAADF images synchronously acquired with a hyperspectral image (9×10^4 sequential spectra obtained while scanning the sample). A series of five emission lines at 5.30, 5.46, 5.62, 5.75, and 5.86 eV are clearly visible in the overall cathodoluminescence spectrum of the nanoparticle (Figure 1c). These energies correspond to previously reported values for h-BN crystals and multiwalled BN nanotubes.[6,18] Photoluminescence experiments conducted at different temperatures show finer structures for temperatures below 50 K.[18] These additional features are smeared at higher temperature and thus are not visible through our experimental set up operating at about 150 K.

The three example spectra presented in Figure 1c show the strong inhomogeneities in the peak's relative intensities occurring at different probe positions. In order to extract the spectral weight of individual emission lines, a multi-Lorentzian fitting routine has been applied to each spectrum of the spectrum image. Whereas peak energies were free parameters of the fitting procedure, no relevant energy shifts were detected across individual and between different flakes. Intensity maps derived from this analysis are shown in Figure 1d–h. Each map has been normalized independently on the basis of the most intense pixel. It should be mentioned however that peaks at 5.62 and 5.86 eV are systematically significantly weaker than other emission lines and this behavior can not be attributed solely to detection efficiency differences.

A detailed analysis of intensity maps demonstrates strong inhomogeneities occurring at lines crossing the flakes. The free excitonic emission at 5.75 eV and the two emission peaks at 5.62 and 5.86 eV are distributed all across the particle. Contrarily, the two emission peaks at 5.30 and 5.46 eV are mostly localized at the lines. All emission maps are clearly not correlated one with another and thus all five emission features should be considered independent. This behavior is strongly visible in very thin h-BN flakes where individual emission lines can be easily spatially separated (Figure 2). In extended regions of these few layer flakes solely occurs the 5.75 eV emission line characteristic of perfect h-BN crystals.

Lines visible in CL maps appear also clearly in HAADF and bright field images and thus they are associated with local structural changes (Figures 1a,b and 2a). Furthermore, they occur mostly in pairs separated by few up to hundred of

dx.doi.org/10.1021/ph500141j | ACS Photonics 2014, 1, 857–862

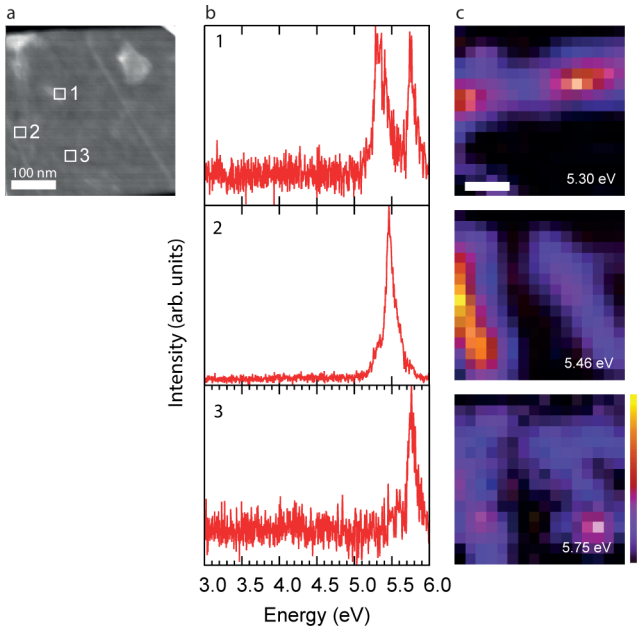

Figure 2. (a) HAADF image of a thin h-BN flake. (b) Spectra extracted from a cathodoluminescence hyperspectral image for probe positions 1−3 indicated in the HAADF image. (c) Cathodoluminescence emission maps of the 5.30, 5.46, and 5.75 eV emission peaks.

nanometers (Supporting Information, Figure 2). For a better understanding on how specific emission peaks are associated with specific structural features, these lines have been characterized by bright field imaging in an aberration corrected STEM.

In Figure 3g we present a HAADF image for a pair of parallel bright lines and the corresponding scanning transmission bright field focal series (Figure 3a−f). Each line is formed by two parallel fringes indicating layers parallel to the electron beam direction. The under-focused image (Figure 3a) is rather similar to the image of a double walled BN nanotube, but unlike the case of a nanotube the focus for the two series of fringes occurs at two different defocus values (Figure 3b,c). This corresponds to a situation where the two series of fringes lie at different depths. Finally when both pairs of fringes are overfocused the image of the underlying h-BN lattice is recovered (Figure 3e,f). A similar behavior is found also for structures with a higher number of fringes (Supporting Information, Figure 3).

The behavior described here can be explained by a model in which a layer stack can deform forming two almost parallel folds (see Figure 4). This double-folded structure has been proposed to occur in neutron irradiated graphite[19] and it has been recently imaged in CVD grown few-layer graphene[20,21] and MoS_2 flakes.[22] Local layer folding is also an extremely common defect occurring in the early stage of hexagonal to cubic BN transformation through high pressure and temperature methods.[23] Emission peaks at energies of 5.30 and 5.46 eV are thus solely associated with folds. Our observations do not allow to exclude the additional presence of single folds, whereas they might be less common than double folds. Emission peaks at energies of 5.30 and 5.46 eV are thus solely associated with folds.

The different curvature of the layers at the fold induces, as for any multi layered structure, a relative glide of the layers and thus a loss of the original AA′ stacking sequence of the perfect h-BN crystal (Figure 4). The local atomic structure of the folds is thus analogous to the structure of multi walled nanotubes where in principle no defined stacking sequence exists. However, in multiwalled BN nanotubes and in other inorganic nanotubes the competition between bending and interplane energies tends to localize the curvature and to promote polygonal tube sections with facets of well-defined stacking, not necessarily AA′.[24−26] The local atomic structure at the fold's facets should thus

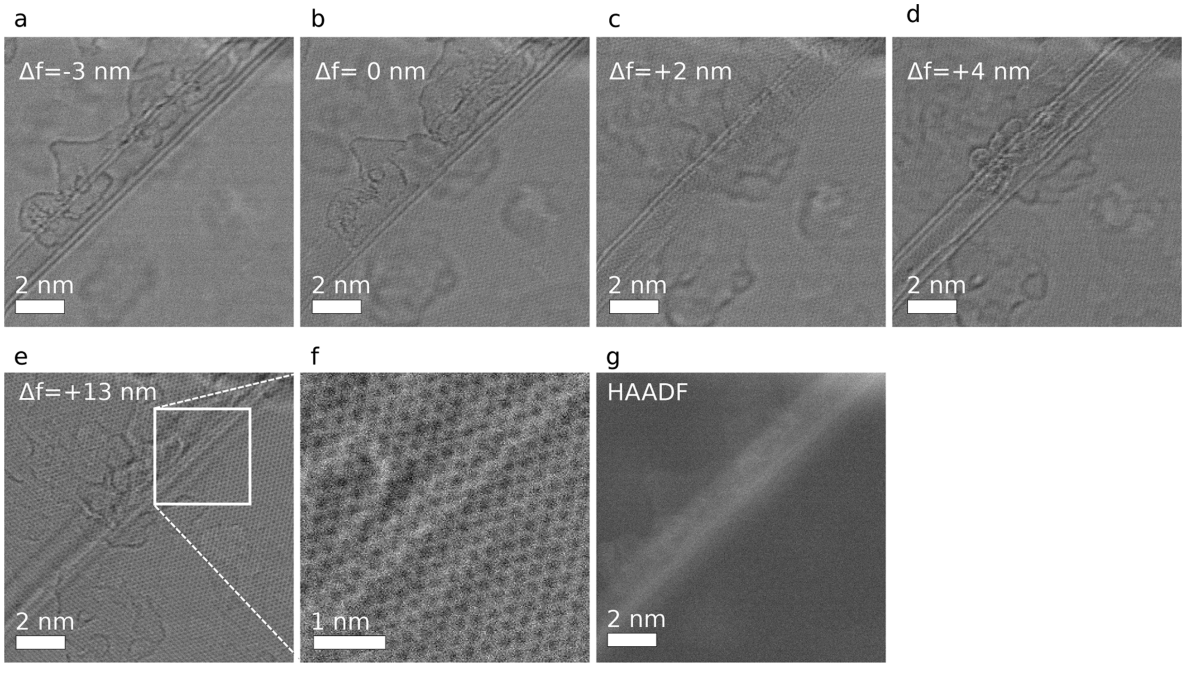

Figure 3. (a−e) Five micrographs of a couple of parallel fringes extracted from a 34-image focal series. The two pair of fringes are focused at different focal depths. (f) Magnified image showing that the fringes are aligned along an arm-chair direction of the h-BN lattice. (g) Dark field image of the region showing a local increase of the projected density at the fold.

dx.doi.org/10.1021/ph500141j | ACS Photonics 2014, 1, 857−862

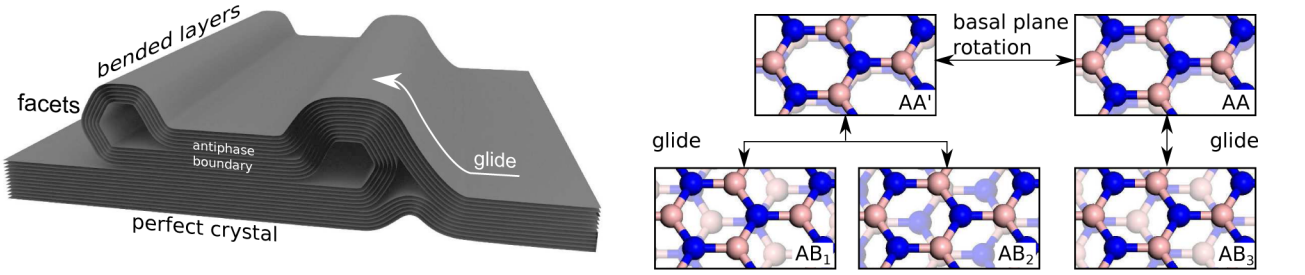

Figure 4. (Left) Model of a faceted double fold in a h-BN crystal. At different sections of the crystal layers glides and antiphase boundaries appear. (Right) Morphological deformations promote transition to different stacking sequences. Layers glide at bended regions transforms the original AA′ stacking in the AB_1 or AB_2 stackings. AA and AB_3 are associated with antiphase boundaries in overlapping regions.

correspond to stacking sequences that can be generated from the original AA′ structure by a glide of the layers. Two high symmetry configurations can then be produced by translating one of the basal planes by a vector $t\cdot(1/3, 2/3, 0)$, with t a real number. For $t = 1$, the AB_1 structure is obtained, where, following an analogous nomenclature for graphite, nitrogen and boron atoms lies at α and β sites, respectively, and for $t = 2$, the AB_2 structure, where atoms positions are inverted (Figure 4). These AB type stacking configurations have been theoretically discussed several times in the literature[27−30] and recently observed by transmission electron microscopy.[31] If the fold follows an armchair direction, as it is seen most often in scanning transmission bright field images (Figure 3e,f), antiphase domains appear in the region between the folds. The stacking of planes at antiphase domain boundaries corresponds to a high symmetry AA order or, by applying an additional translation, an AB_3 order (Figure 4). Besides the specific fold case, antiphase domains are, as for graphite, a common defect in h-BN and indeed AA stacking orders, stabilized by intercalated atoms, have been recently identified in few layer h-BN crystals.[32]

These topological considerations suggest that additional excitonic peaks should be associated solely with changes of the crystal symmetry in the above-mentioned five high symmetry stacking sequences. In order to confirm this hypothesis we have performed a complementary theoretical investigation of the optical spectra for these configurations. It has been successfully demonstrated that fundamental insights on emission can be provided by an analysis of simulated absorption spectra, taking into account that absolute energies could not be accessed due to the neglect of Stokes shifts.[4,9,18] Wave functions were obtained in the framework of density functional theory using the local density approximation and quasi particle energies were corrected by a subsequent GW treatment.[33] In a first step, optical spectra were evaluated in the random phase approximation (RPA). Finally, electron hole interactions, associated with excitonic effects that dominate the h-BN optical spectra, have been included by solving the Bethe-Salpeter equation[34] (BSE). This computational scheme has been successfully applied to the study of the absorption spectrum of h-BN and BN nanotubes.[4,9,35,36] Due to the well-known underestimation of the h-BN band gap in the non self-consistent GW computational scheme a 0.35 eV rigid shift has been applied to all spectra that allows the alignment of the excitonic peak of the AA′ stacking to the known experimental value.

For different h-BN polytypes, there are strong changes in the band dispersion observed both at the DFT and GW level and in particular in out of plane reciprocal space directions where direct gaps are minimal (see Table 1 in the Supporting Information and ref 27). This behavior has also a fundamental role in defining the optical properties of different stacking configurations. Indeed in agreement with the work of Arnaud et al. on AA′ h-BN,[8] we find for all configurations that directions parallel to the c^* axis give rise to the first absorption peak of ε_2 both at RPA and BSE levels. Quasi-particle band gaps and exciton binding energies are finally strongly dependent on the stacking order and determine the energies of optically active excitons (more details will be provided in a future work).

All absorption spectra presented in Figure 5 show strong excitons with well separated energies in the range between 5.2

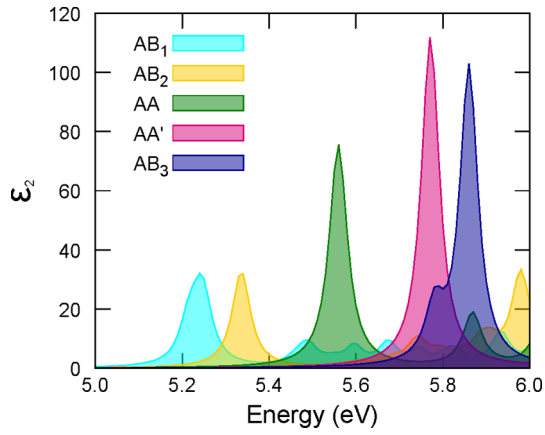

Figure 5. Imaginary part of the dielectric function (optical absorption spectrum) for different h-BN stacking obtained in the framework of GW + BSE calculations.

to 5.9 eV depending on the stacking configuration. Taking as a reference the standard AA′ exciton at 5.75 eV, three additional excitons, associated with the AB_1, AB_2 and AA configurations, occur at lower energies whereas that of the AB_3 configuration is found at a higher one. Energy range and peak distribution coincide with experimental results. Thus, theoretical simulations enable us to associate each of the five measured emission peaks with the five high symmetry configurations analyzed. In particular, emissions at 5.30 and 5.46 eV, strongly localized at folds, can be attributed to AB_1 and AB_2 stacking sequences, respectively. These models are compatible with the faceted fold structure where discrete layer glides between facets give rise to well-defined stacking orders. Emissions at 5.62 and 5.86 eV can be associated with the AA and AB_3 stacking, respectively. Since these stackings appear at antiphase boundaries, these excitons occur in large regions of the flake and their signal is weak due to the small number of atomic planes involved. We underline that

dx.doi.org/10.1021/ph500141j | ACS Photonics 2014, 1, 857−862

each intermediate stacking gives rise to different exciton energies (Supporting Information, Figure 4). The experimental evidence for only five discrete emission lines is thus a clear indication of a finite number of stacking configurations and it confirms the hypothesis of faceted folds.

CONCLUSIONS

In this work, using a complementary experimental and theoretical approach we have provided a microscopic explanation for the complex emission spectrum of h-BN relating local changes in the layer stacking order to the appearance of additional excitons. Furthermore, we have shown how these defects and the associated excitonic emissions can be strongly localized at folds crossing the flakes. The local structure of these extended defects can be related to local symmetry changes due to stacking faults. Metastable h-BN stackings have been discussed from a morphological and energetic point of view, but little attention was paid to their optical and electronic properties.[27−30] Only recently it has been demonstrated that few layer h-BN structures with noncentrosymmetric configurations (flakes with odd number of layers or twisted bilayer flakes) have remarkable second harmonic generation and thus a great potential for nonlinear optics applications.[37−39] In this study we emphasizes the role of stacking changes in h-BN flakes in defining the specific optical response in the ultraviolet regime.

Stacking faults in layered materials are natively abundant due to their low activation energy and they can be easily induced by limited mechanical deformations. Futhermore, recent developments in 2D crystals transfer techniques allow to build multilayer structures with arbitrary stacking orientations.[38,40] This study suggests that deliberately introducing stacking faults in h-BN flakes can be used as a way to tune the emission spectrum in the far UV region. From a complementary point of view, the analysis of the excitonic response can be employed as a powerful tool to precisely map structural deformations in h-BN crystallites and in new 2D heterostructures.

METHODS

Synthesis. Few-layer hexagonal boron nitride flakes was obtained by chemical exfoliation of commercially available micrometric powder following the protocol presented in ref 41. A solution of 10 mg of h-BN powder in 10 mL of isopropanol was sonicated for 7 h and subsequently centrifuged for 120 min at 500 rpm. The supernatant was then dropped onto a TEM copper grid. Samples were then purified by a 3 h at 500 °C thermal treatment in a 800 mbar forming gas atmosphere (95% N_2, 5% H_2). HREM images and core level electron energy loss spectroscopy confirmed the absence of any carbon contamination due to solvent residuals. Flakes presented a lateral size of few microns.

Microscopy and Spectroscopy. Cathodoluminescence was performed in a dedicated VG-HB501 scanning transmission electron microscope operating at 60 keV, below the atomic displacement threshold for h-BN in order to avoid irradiation damage.[42,43] Optical spectra were collected using an optical spectrometer with a 300 groove diffraction grating blazed at 300 nm. The resolution of the CCD was 0.17 nm/pixel.

High resolution scanning transmission electron microscopy images were recorded in a NION ULTRA-STEM 200 microscope operating at 60 keV. Lattice planes were visible in bright field images but not in dark field due to the resolution loss at low voltage and the rather high thickness and orientation complexity of the sample.

Computational Details. Quantum mechanical calculations of electronic and optical properties for the five stacking configurations of bulk h-BN were performed following a well established computational procedure. Ground state electronic structures were derived using plane waves pseudopotential density functional theory as implemented in the Abinit package within the local density approximation (LDA). A Monkhorst-pack grid of 10 × 10 × 4 *k*-point was used to sample the Brillouin zone of the system. An energy cutoff of 32 Ha was demonstrated to be enough for the convergence of the total energy. Following the ground state calculations, self-energy corrections to the Kohn−Sham eigenvalues for high symmetry points of the Brillouin zone was obtained using many body perturbation theory (MBPT) adopting a non-self-consistent GW approach. The 6 × 6 × 2 *k*-grid for GW calculations was not shifted meaning that the gamma point was included.

In a first step, optical spectra were evaluated in the random phase approximation (RPA). Dielectric functions were derived using a 15 × 15 × 7 shifted *k*-grid and 30 energy bands. Crystal local field effects were included (with 50 G vectors) and for each configuration a scissor operator was applied by using the corresponding GW self-energy correction. Since for all structures the dispersion of the GW correction was lower than 0.5 eV, the scissor operator for different stackings was chosen as the corresponding GW correction at gamma.

In a second step, we performed optical spectra calculations by using the Bethe-Salpeter equation, which permits to include electron−hole interaction by mixing all the electronic transitions in the resolution of a two particle equation. A 15 × 15 × 7 shifted *k*-grid was used, with 50 G-vectors and a broadening of 0.025 eV.

ASSOCIATED CONTENT

Supporting Information

Full emission spectrum of h-BN, complementary cathodoluminescence and HREM images, and theoretical spectra for additional stacking configurations. This material is available free of charge via the Internet at http://pubs.acs.org.

AUTHOR INFORMATION

Corresponding Author

*E-mail: alberto.zobelli@u-psud.fr.

Notes

The authors declare no competing financial interest.

ACKNOWLEDGMENTS

The authors acknowledge support from the Agence Nationale de la Recherche (ANR), program of future investment TEMPOS-CHROMATEM (No. ANR-10-EQPX-50), and Triangle de la Physique, Theo-STEM Project (No. 2010-085T). The work has also received funding from the European Union in Seventh Framework Programme (No. FP7/2007-2013) under Grant Agreement No. n312483 (ESTEEM2) and Marie Curie Intra-European Fellowship No. 326794 (EXPRESS).

REFERENCES

(1) Taniyasu, Y.; Kasu, M.; Makimoto, T. An aluminium nitride light-emitting diode with a wavelength of 210 nanometres. *Nature* **2006**, *441*, 325−328.

(2) Khan, A.; Balakrishnan, K.; Katona, T. Ultraviolet light-emitting diodes based on group three nitrides. *Nat. Photonics* **2008**, *2*, 77−84.
(3) Watanabe, K.; Taniguchi, T.; Kanda, H. Direct-bandgap properties and evidence for ultraviolet lasing of hexagonal boron nitride single crystal. *Nat. Mater.* **2004**, *3*, 404−409.
(4) Wirtz, L.; Marini, A.; Gruning, M.; Rubio, A. Excitonic effects in optical absorption and electron-energy loss spectra of hexagonal boron nitride. *arXiv:cond-mat/0508421* **2005**,.
(5) Jaffrennou, P.; Donatini, F.; Barjon, J.; Lauret, J.-S.; Maguer, A.; Attal-Tretout, B.; Ducastelle, F.; A, L. Cathodoluminescence imaging and spectroscopy on a single multiwall boron nitride nanotube. *Chem. Phys. Lett.* **2007**, *442*, 372−375.
(6) Jaffrennou, P.; Barjon, J.; Schmid, T.; Museur, L.; Kanaev, A.; Lauret, J.-S.; Zhi, C. Y.; Tang, C.; Bando, Y.; Golberg, D.; Attal-Tretout, B.; Ducastelle, F.; Loiseau, A. Nearband-edge recombinations in multiwalled boron nitride nanotubes: Cathodoluminescence and photoluminescence spectroscopy measurements. *Phys. Rev. B* **2008**, *77*, 235422.
(7) Watanabe, K.; Taniguchi, T.; Niiyama, T.; Miya, K.; Taniguchi, M. Far-ultraviolet plane-emission handheld device based on hexagonal boron nitride. *Nat. Photonics* **2009**, *3*, 591−594.
(8) Arnaud, B.; Lebégue, S.; Rabiller, P.; Alouani, M. Huge excitonic effects in layered hexagonal boron nitride. *Phys. Rev. Lett.* **2006**, *96*, 026402.
(9) Wirtz, L.; Marini, A.; Grüning, M.; Attaccalite, C.; Kresse, G.; Rubio, A. Comment on huge excitonic effects in layered hexagonal boron nitride. *Phys. Rev. Lett.* **2008**, *100*, 189701.
(10) Kubota, Y.; Watanabe, K.; Tsuda, O.; Taniguchi, T. Deep ultraviolet light-emitting hexagonal boron nitride synthesized at atmospheric pressure. *Science* **2007**, *317*, 932−934.
(11) Museur, L.; Anglos, D.; Petitet, J.-P.; Michel, J.-P.; Kanaev, A. V. Photoluminescence of hexagonal boron nitride: Effect of surface oxidation under UV-laser irradiation. *J. Lumin.* **2007**, *127*, 595−600.
(12) Museur, L.; Feldbach, E.; Kanaev, A. Defect-related photoluminescence of hexagonal boron nitride. *Phys. Rev. B* **2008**, *78*, 155204.
(13) Watanabe, K.; Taniguchi, T.; Kuroda, T.; Kanda, H. Band-edge luminescence of deformed hexagonal boron nitride single crystals. *Diamond Relat. Mater.* **2006**, *15*, 1891−1893.
(14) Watanabe, K.; Taniguchi, T.; Kuroda, T.; Kanda, H. Effects of deformation on bandedge luminescence of hexagonal boron nitride single crystals. *Appl. Phys. Lett.* **2006**, *89*, 141902.
(15) Jaffrennou, P.; Barjon, J.; Lauret, J. S.; Attal-Trétout, B.; Ducastelle, F.; Loiseau, A. Origin of the excitonic recombinations in hexagonal boron nitride by spatially resolved cathodoluminescence spectroscopy. *J. Appl. Phys.* **2007**, *102*, 116102.
(16) Pierret, A.; Loayza, J.; Berini, B.; Betz, A.; Plaçais, B.; Ducastelle, F.; Barjon, J.; Loiseau, A. Excitonic recombinations in h-BN: From bulk to exfoliated layers. *Phys. Rev. B* **2014**, *89*, 035414.
(17) Zagonel, L. F.; Mazzucco, S.; Tence, M.; March, K.; Bernard, R.; Laslier, B.; Jacopin, G.; Tchernycheva, M.; Rigutti, L.; Julien, F. H.; Songmuang, R.; Kociak, M. Nanometer scale spectral imaging of quantum emitters in nanowires and its correlation to their atomically resolved structure. *Nano Lett.* **2010**, *11*, 568−573.
(18) Watanabe, K.; Taniguchi, T. Jahn-Teller effect on exciton states in hexagonal boron nitride single crystal. *Phys. Rev. B* **2009**, *79*, 193104.
(19) Heggie, M. I.; Suarez-Martinez, I.; Davidson, C.; Haffenden, G. Buckle, ruck and tuck: A proposed new model for the response of graphite to neutron irradiation. *J. Nucl. Mater.* **2011**, *413*, 150−155.
(20) Robertson, A. W.; Bachmatiuk, A.; Wu, Y. A.; Schäffel, F.; Büchner, B.; Rümmeli, M. H.; Warner, J. H. Structural distortions in few-layer graphene creases. *ACS Nano* **2011**, *5*, 9984−9991.
(21) Kim, K.; Lee, Z.; Malone, B. D.; Chan, K. T.; Aleḿan, B.; Regan, W.; Gannett, W.; Crommie, M. F.; Cohen, M. L.; Zettl, A. Multiply folded graphene. *Phys. Rev. B* **2011**, *83*, 245433.
(22) Castellanos-Gomez, A.; Roldán, R.; Cappelluti, E.; Buscema, M.; Guinea, F.; Van der Zant, H. S. J.; Steele, G. A. Local strain engineering in atomically thin MoS_2. *Nano Lett.* **2013**, *13*, 5361−5366.
(23) Nistor, L.; Van Tendeloo, G.; Dinca, G. Crystallographic aspects related to the high pressure−high temperature phase transformation of boron nitride. *Philos. Mag.* **2005**, *85*, 1145−1158.
(24) Celik-Aktas, A.; Zuo, J.-M.; Stubbins, J. F.; Tang, C.; Bando, Y. Double-helix structure in multiwall boron nitride nanotubes. *Acta Cryst. A* **2005**, *61*, 533−541.
(25) Tibbetts, K.; Doe, R.; Ceder, G. Polygonal model for layered inorganic nanotubes. *Phys. Rev. B* **2009**, *80*, 014102.
(26) Golberg, D.; Mitome, M.; Bando, Y.; Tang, C.; Zhi, C. Multi-walled boron nitride nanotubes composed of diverse cross-section and helix type shells. *Appl. Phys. A: Mater. Sci. Process.* **2007**, *88*, 347−352.
(27) Liu, L.; Feng, Y.; Shen, Z. Structural and electronic properties of h-BN. *Phys. Rev. B* **2003**, *68*, 104102.
(28) Marom, N.; Bernstein, J.; Garel, J.; Tkatchenko, A.; Joselevich, E.; Kronik, L.; Hod, O. Stacking and registry effects in layered materials: the case of hexagonal boron nitride. *Phys. Rev. Lett.* **2010**, *105*, 046801.
(29) Yin, J.; Hu, M.; Yu, Z.; Zhang, C.; Sun, L.; Zhong, J. Direct or indirect semiconductor: The role of stacking fault in h-BN. *Physica B* **2011**, *406*, 2293−2297.
(30) Constantinescu, G.; Kuc, A.; Heine, T. Stacking in bulk and bilayer hexagonal boron nitride. *Phys. Rev. Lett.* **2013**, *111*, 036104.
(31) Warner, J. H.; Rummeli, M. H.; Bachmatiuk, A.; Buchner, B. Atomic resolution imaging and topography of boron nitride sheets produced by chemical exfoliation. *ACS Nano* **2010**, *4*, 1299−1304.
(32) Shmeliov, A.; Kim, J. S.; Borisenko, K. B.; Wang, P.; Okunishi, E.; Shannon, M.; Kirkland, A. I.; Nellist, P. D.; Nicolosi, V. Impurity induced non-bulk stacking in chemically exfoliated h-BN nanosheets. *Nanoscale* **2013**, *5*, 2290−2294.
(33) Hedin, L. New method for calculating the one-particle Green's function with application to the electron-gas problem. *Phys. Rev.* **1965**, *139*, A796−A823.
(34) Onida, G.; Reining, L.; Rubio, A. Electronic excitations: density-functional versus many-body Green's-function approaches. *Rev. Mod. Phys.* **2002**, *74*, 601−659.
(35) Attaccalite, C.; Bockstedte, M.; Marini, A.; Rubio, A.; Wirtz, L. Coupling of excitons and defect states in boron-nitride nanostructures. *Phys. Rev. B* **2011**, *83*, 144115.
(36) Galambosi, S.; Wirtz, L.; Soininen, J. A.; Serrano, J.; Marini, A.; Watanabe, K.; Taniguchi, T.; Huotari, S.; Rubio, A.; Hämäläinen, K. Anisotropic excitonic effects in the energy loss function of hexagonal boron nitride. *Phys. Rev. B* **2011**, *83*, 081413.
(37) Li, Y.; Rao, Y.; Mak, K. F.; You, Y.; Wang, S.; Dean, C. R.; Heinz, T. F. Probing symmetry properties of few-layer MoS_2 and h-BN by optical second-harmonic generation. *Nano Lett.* **2013**, *13*, 3329−3333.
(38) Kim, C.-J.; Brown, L.; Graham, M. W.; Hovden, R.; Havener, R. W.; McEuen, P. L.; Muller, D. A.; Park, J. Stacking order dependent second harmonic generation and topological defects in h-BN bilayers. *Nano Lett.* **2013**, *13*, 5660−5665.
(39) Grüning, M.; Attaccalite, C. Second harmonic generation in BN and MoS_2 monolayers: Role of electron-hole interaction. *Phys. Rev. B* **2014**, *89*, 081102.
(40) Castellanos-Gomez, A.; Buscema, M.; Molenaar, R.; Singh, V.; Janssen, L.; van Herre, S. J. d. Z.; Steele, G. A. Deterministic transfer of two-dimensional materials by all-dry viscoelastic stamping. *2D Materials* **2014**, *1*, 011002.
(41) Coleman, J. N.; et al. Two-dimensional nanosheets produced by liquid exfoliation of layered materials. *Science* **2011**, *331*, 568−571.
(42) Zobelli, A.; Gloter, A.; Ewels, C. P.; Seifert, G.; Colliex, C. Electron knock-on cross section of carbon and boron nitride nanotubes. *Phys. Rev. B* **2007**, *75*, 245402.
(43) Kotakoski, J.; Jin, C. H.; Lehtinen, O.; Suenaga, K.; Krasheninnikov, A. V. Electron knock-on damage in hexagonal boron nitride monolayers. *Phys. Rev. B* **2010**, *82*, 113404.